Isothermal aging characteristics of rare earth magnesium hexaaluminate based advanced thermal barrier coatings

Premanshu Jana[1,2], Ponnarassery S Jayan[2], Santanu Mandal[3] and Koushik Biswas[1]*

[1]*Department of Metallurgical and Materials Engineering, Indian Institute of Technology, Kharagpur 721302, India*
[2]*Electro Minerals Division, Carborundum Universal Limited, Kochi 683109, India*
[3]*Industrial Ceramics Division, Carborundum Universal Limited, Hosur 635126, India*

*Corresponding author

DOI: 10.5185/amlett.2018.1674
www.vbripress.com/aml

Abstract

The isothermal aging characteristics of rare earth magnesium hexaaluminate (REMHA) based thermal barrier coatings (TBC) such as lanthanum magnesium hexaaluminates (LMHA), Neodymium doped LMHA (LNMHA) and LNMHA-Yttrium aluminium garnet (YAG) composite were evaluated at 1400°C and compared with standard yttria stabilized zirconia (YSZ) coating. The platelet structure of hexaaluminate forms meso-porous structure and provides superior sintering resistance than YSZ coating. Faster grain growth kinetics is observed in YSZ coating as compared to hexaaluminate-based coatings. As a result, the mechanical properties of YSZ coating deteriorate severely whereas hexaaluminate based coating remains almost unaltered. The LNMHA coating is found to be the best sintering resistance among them. LNMHA and LNMHA-YAG composite have potential to meet the requirement of advanced TBC operating even at 1400°C. Copyright © 2018 VBRI Press.

Keywords: Grain growth, microstructure-final, platelet, mechanical properties, isothermal ageing.

Introduction

The thermal barrier coatings (TBC) are used primarily to protect the hot section components of gas turbine from excessive heat and high temperature corrosion [1-3]. A thin layer of coatings provides a thermal insulation and maintains the surface temperature of the super alloy blade well below its melting points. TBC mainly consists of two different layers i.e., a metallic bond coat over super alloy followed by a ceramic top coat. A layer of aluminum oxide is grown over a period of time in between them over a period of time which is known as thermally grown oxide (TGO) [1, 4]. The most commonly used ceramic top coat is 7-8 wt. % yttria stabilized zirconia (YSZ) which function well up to 1200°C [5, 6]. The ever increasing demand of higher gas turbine efficiency leads to a higher operating temperature i.e., higher gas inlet temperature. There is a significant advancement of the superalloy as well as cooling system over the years. The inlet temperature is started approaching towards 1650°C [7].As the operating temperature goes beyond 1200°C, YSZ coating fails the stringent requirement of advanced TBC. The major disadvantages of YSZ are phase changes, accelerated sintering, severe hot corrosion etc. which leads to a premature failure of TBC [6, 8]. The demand for advanced TBC materials that can operate at elevated temperature at least 1400°C is very high.

The basic requirements of advanced TBC are low thermal conductivity (TC, <2.3 W/mK), high thermal expansion coefficient (CTE, ~10.5 × 10^{-6}/K), no phase transformation, no oxygen transparency etc., [9, 10]. Several materials are proposed as ceramic top coat during last decades. Out of them, rare earth magnesium hexaaluminates especially lanthanum magnesium hexaaluminate ($LaMgAl_{11}O_{19}$) emerge as one of the most promising alternate for advanced TBC [11-13]. It has good thermo-physical properties and also has potential to meet the requirement advanced TBC [13, 14].

Degradation of ceramic top coat due to excessive sintering, phase transformation at the service temperature is one of the major drawbacks of the existing YSZ when operating temperature goes beyond 1200°C [15-18]. The porous microstructure of the coating gets changed over a prolong service period which results in the change in thermophysical properties, strain tolerance capability etc. [15, 18, 19]. They can cause a premature failure of the TBC. Therefore, the thermal stability of ceramic top exposed to the high temperature for longer duration is one of the important aspects. Isothermal aging characteristics of these materials at elevated temperature (>1200°C) are very limited.

Therefore, the investigation isothermal aging characteristics at elevated temperature (at 1400°C) of the potential REMHA based TBC materials are highly

relevant and extensively studied in this present work. Isothermal aging characteristics of standard YSZ coating are also investigated in similar conditions to compare the new TBC materials with the standard.

Experimental

Material synthesis

The lanthanum magnesium hexaaluminate ($LaMgAl_{11}O_{19}$), neodymium doped LMHA ($La_{0.5}Nd_{0.5}MgAl_{11}O_{19}$) and LNMHA-YAG composite were prepared by an advanced sol-gel processing [20, 21]. Boehmite, magnesium nitrate, lanthanum nitrate, neodymium nitrate and yttrium nitrate were used as a source of alumina, magnesia, lanthana, neodymia and yttrium respectively. These precursors are commercially available and used as such without any purification (Purity ~99.95%). The detailed processing is reported elsewhere [20, 22].

Isothermal aging

Thick coatings of these materials were prepared by atmospheric plasma spraying on graphite block. Plasma spraying conditions are summarized in **Table 1**. Free standing ceramic top coats were obtained by removing the graphite block in a muffle furnace at 750°C for 2h. The free standing coating was sectioned and used for the isothermal aging study. The specimens were heated in the muffle furnace (in air) at 1400°C for different duration up to 100h. The heating rate was maintained at 5°C/min. Specimens were cooled inside the furnace and taken out for evaluation.

Table 1. Plasma spraying conditions for TBC formation on graphite block.

Type of Coating	Spray distance (mm)	Voltage (V)	Current (A)	Plasma gas, Ar/H_2 (NLPM)	Carrier gas, Ar (NLPM)	Powder feed rate (g/min)	Coating thickness (μm)
Top coat	120	80	600	35/12	3.4	30	1000±50

Characterizations techniques

Density of the free standing coatings was measured by Archimedes' principle using boiling water method (ASTM standard C20-00). The thermal behaviour of the dry gel was studied upto 1500°C in air by simultaneous thermo gravimetric (TG) and differential thermal analysis (DTA) instrument (Netzsch, Germany). The heating rate was maintained at 10°C/min. Phase analysis was done using X-ray diffractometer (XRD) (Bruker AXS, D8 Advance, Germany) using Ni filtered CuK_α radiation (λ = 0.15405 nm). The step size and the scan rate were maintained at 0.02° (2θ) and 3°/min respectively. The micrographs of the isothermally aged samples were obtained by a scanning electron microscope (SEM) attached with energy dispersive x-ray spectra (EDS) (JEOL, Japan).

Mechanical properties of the free standing coatings were measured by indentation tests. The vicker's micro-hardness tester interfaced with computer (Shimadzu, HMV, Japan) was used for the measurement. The samples were mounted in epoxy resin and polished using SiC water papers followed by 1-3 micron diamond paste. The polished samples were was cleaned thoroughly and dried prior to test. The micro-hardness of the sample was obtained from the indentation diagonal of vicker's indenter. Fracture toughness was calculated from the crack length of an indentation using Anstis formula [23]. Elastic modulus was obtained from Knoop indentation using Marshall's equations [24]. The test load for micro-hardness, fracture toughness and Knoop indentation was 2.94 N, 9.8 N and 2.94 N respectively. 8-10 measurements were taken to obtain an average value and error bar was calculated from the standard deviation.

Results and discussion

As sprayed TBCs

Thermal analysis

TG-DSC graphs of four different TBCs are shown **Fig. 1**. The weight of all the TBCs remains almost constant. The marginal weight loss could be due to the burning of residual carbon as free standing coating was formed on graphite surface and the DSC sample was prepared by abrading the graphite layer. On the other hand weight gain could be due to the oxidation of trace metallic contamination during formation of coatings.

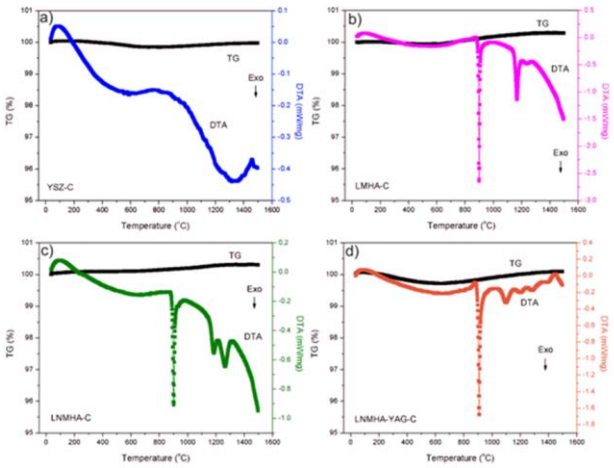

Fig. 1: TG-DSC curves of (a) YSZ, (b) LMHA, (c) LNMHA and (d) LNMHA-YAG coating.

DSC curve of YSZ shows a broad exothermic peak centered around 1345 °C which could be due to the phase transition of monoclinic to tetragonal zirconia. A trace amount of monoclinic zirconia may have been present along with the metastable tetragonal zirconia which can be confirmed by XRD result discussed later. The DSC curves of all three hexaaluminates show almost similar trend. The DSC curve of LMHA shows two strong exothermic peaks observed at 900 °C and 1170 °C. The TBC formed by APS process generally have significant amount of amorphous phase as molten splats solidify very fast (>10^6 °C/s). The first peak could be due to the crystallization of this amorphous coating, i.e., formation of intermediate phase such as $LaAlO_3$, θ-Al_2O_3. The second peak could be due to the transformation of

Copyright © 2018 VBRI Press

transition alumina (θ-Al_2O_3) to alpha alumina. Similar crystallization phenomena were observed for LMHA at lower temperature for LMHA [25]. The APS process also causes decomposition of LMHA into basic components as shown in equation 1 [26].

$$LaMgAl_{11}O_{19} = LaAlO_3 + MgO + 5Al_2O_3 \quad (1)$$

The basic constituents react further to form the rare earth hexaaluminate during heating. The tiny peak (third peak) observed at 1245 °C may correspond to the formation of the LMHA phase.

In case of LNMHA coating, the first peak appeared at same temperature (900 °C) and second peak shifted to slightly higher temperature, i.e., at 1200 °C. The third peak is relatively strong and observed at 1270 °C. For LNMHA-YAG coating, one more additional peak (fourth peak) is observed at 1100 °C and is attributed to the formation of garnet phase.

Phase analysis

Fig. 2 shows the XRD patterns of the coatings heat treated at different temperatures. The TBC made of standard YSZ is well crystalline and has metastable tetragonal phases along with a small amount of monoclinic phase (~3.5%) (**Fig. 2a,** 750 °C-2 h). This is in agreement with the DSC result. On the other hand, LMHA, LNMHA and LNMHA-YAG coatings are primarily amorphous in nature. Tiny peaks corresponding to the LMHA are seen for all the samples. Additional phases like YAG and YAM are present along with LMHA phase for LNMHA-YAG composite. These minor crystalline phases could arise from the un-melted or semi-melted particles of the feed material deposited during coating formation.

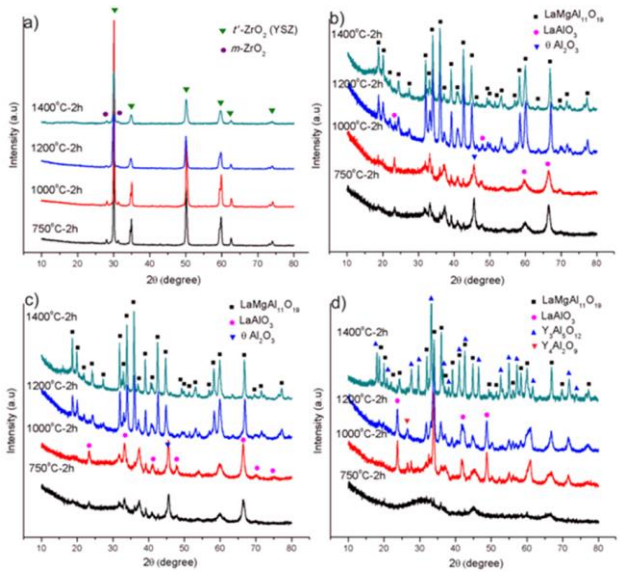

Fig. 2. XRD patterns of heat treated coatings at different temperatures for 2 h; a) YSZ, b) LMHA, c) LNMHA and d) LNMHA-YAG.

The crystallization of these amorphous coatings takes place during heat treatment and shows several intermediate phase formation before arriving at the final phases. This is in well agreement with the DSC results. The coatings remain amorphous till 750 °C and crystallize into intermediate phase like LMA, transition alumina and YAM at 1000 °C. However, full crystallization for LMHA and LNMHA coatings to their final phase is observed at 1200 °C for 2 h. The intermediate phases are almost disappeared. On the other hand, the intermediate phases are present in LNMHA-YAG coating as a major phase along with the LMHA and YAG phases, i.e., the phase formation is not completed at 1200 °C for 2 h. The phase pure LNMHA-YAG composite is observed at 1400 °C for 2 h.

Microstructural evaluation

The microstructures of as sprayed coating surface and fracture surface are shown in **Fig. 3**. The surface of as sprayed YSZ coatings **(Fig. 3a)** is relatively rough and contains significant amount of un-melted and semi-melted particles along with the molten splats. There are also micro cracks on the completely melted splat which could be due to the thermal stress generated from the rapid solidification of molten droplets. The fracture surface of YSZ **(Fig. 3b)** shows the typical lamellar structure where micro pores and cracks are present at inter lamellar places. The lamellae are well crystalline and have fine columnar grains. The columnar structure is generally formed by the directional solidification of molten mass which is very obvious for plasma spray coating.

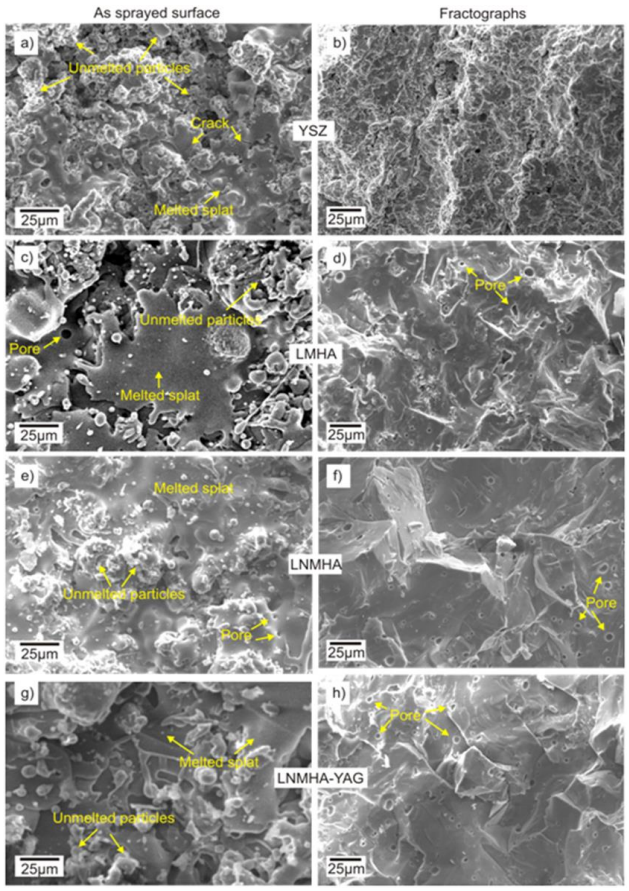

Fig. 3. The microstructure of as sprayed coating surface and fractographs of YSZ, LMHA, LNMHA and LNMHA-YAG.

Copyright © 2018 VBRI Press

All the hexaaluminate based coatings have almost similar surface morphology and are significantly different from YSZ coating. Here, the particles are completely liquefied by plasma flame and the molten splats form a lamellar structure. Small amount of semi-molten and solid un-melted particles are evident but there are no such visible micro cracks seen in the coatings. The overlap lamellar structure enhances the inter lamellae bonding. There are few open pores on the surface which could be due to the release of entrapped gases during solidification of molten splats. The fracture surfaces also reveal the well bonded inter splat structure with few spherical micro pores. These spherical micro pores are formed due to the entrapment of gas which might not be able to escape due to rapid solidification. The good inter lamellae bonding and dispersion of micro pores across the coating thickness are beneficial for the thermal barrier coatings. A good bonding can prevent the inter splat crack propagation whereas micro pores will help to reduce the effective thermal conductivity of the coating. All three hexaaluminate based coatings are amorphous in nature and are in well agreement with the XRD results.

Density of free standing coatings

The relative density of the four different TBCs is given in **Table 2**. It is seen that the relative density of all the coatings is almost similar and varies from 83.93 to 84.96 %. Significant amount of micro cracks, micro pores and flaws are present along with the macro pores in the coating which is clearly evident from the microstructural features. The standard YSZ coating seems to have higher amount of micro cracks and micro pores which could be due to the presence of higher amount of un-melted particles in the coating. On the other hand hexaaluminate based coating contains relatively higher amount of macro pores which could be originated from the entrapped gas during solidification.

Table 2. Relative density of plasma spray coatings.

Sample details	YSZ	LMHA	LNMHA	LNMHA-YAG
Relative density, %	83.93	84.76	84.59	84.96

Mechanical properties

The micro-hardness, fracture toughness and elastic modulus of four different TBCs are shown in **Fig. 4**. These properties are measured on the polished cross section of TBCs. The mechanical properties of hexaaluminate based coatings are significantly higher than that of YSZ. The micro-hardness, fracture toughness and elastic modulus of YSZ coating are 6.31±0.21GPa, 1.77±0.05 MPa·m$^{1/2}$ and 37.54±10.28 GPa, respectively, which are typical properties of plasma sprayed YSZ [27-29].

Higher hardness and fracture toughness will be beneficial for the coatings as higher hardness can contribute to better erosion resistance of the coating and higher toughness can consume more stress energy prior to crack initiation as well as propagation. This is to be noted that the as prayed TBCs based on hexaaluminates are

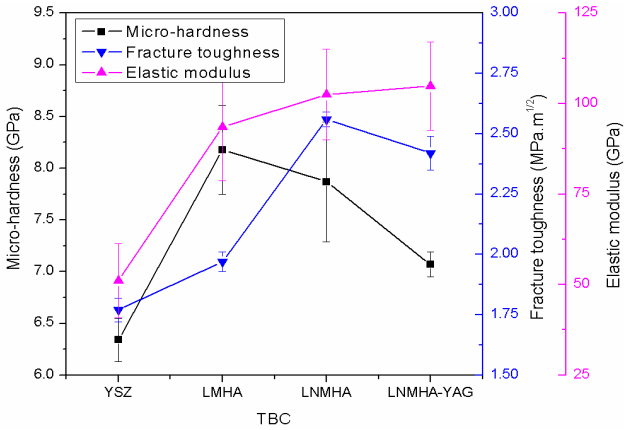

Fig. 4. Micro-hardness, fracture toughness and elastic modulus of as-sprayed TBCs.

amorphous in nature. The mechanical properties of as sprayed coatings are imperative as they experience several changes during heat treatment. The mechanical properties of isothermally aged TBCs are discussed in later section.

Isothermal aging of TBCs

Density and porosity

The variation in density of the free standing coatings, isothermally aged at 1400 °C up to 100 h, are shown in **Fig. 5**. There is a sharp increase in density (~4%) in first 10 h of soaking and then it increases nearly 10% and 4%, respectively in next 90 h of dwelling for YSZ and hexaaluminate based coatings. In the case of YSZ coating, the initial increase in density could be resulted from the annihilation of various defects present in the coatings and the later part could be a result of pure sintering. The porous structures, i.e., inter and intra splat pores as well as micro cracks are eliminated and form a denser structure. As a result, the final density after 100 h of dwelling is reached to around 98% of the theoretical one. It is well known that the sintering of YSZ top coat can cause a substantial increase in thermal conductivity by eliminating micro pores and also reduces the strain tolerance capability in relation with increasing Young's modulus [13, 30]. These changes are detrimental for TBC and can lead to a premature failure.

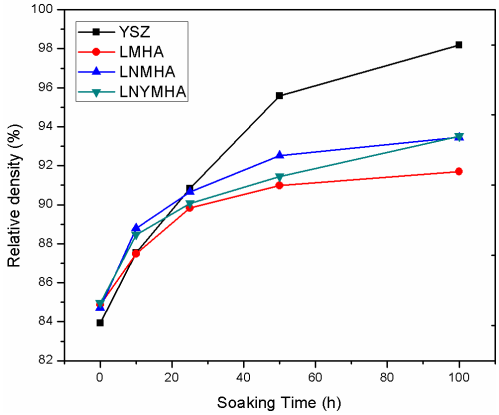

Fig. 5. The variation of relative density of free standing coatings isothermally aged at 1400 °C.

Copyright © 2018 VBRI Press

The initial increase in density of hexaaluminate based coatings is primarily due to crystallization of their amorphous coatings. There could be a little contribution from the defects annihilation. The final densities of LMHA, LNMHA and LNMHA-YAG coatings (after 100 h of dwelling) are 91, 93 and 93%, respectively. The superior sintering resistances of rare earth magnesium hexaaluminates are well known due to their platelets structure. The similar phenomenon is evident here for the hexaaluminate based coatings. The parent LMHA has more sintering resistance than the doped LMHA and LNMHA-YAG composite.

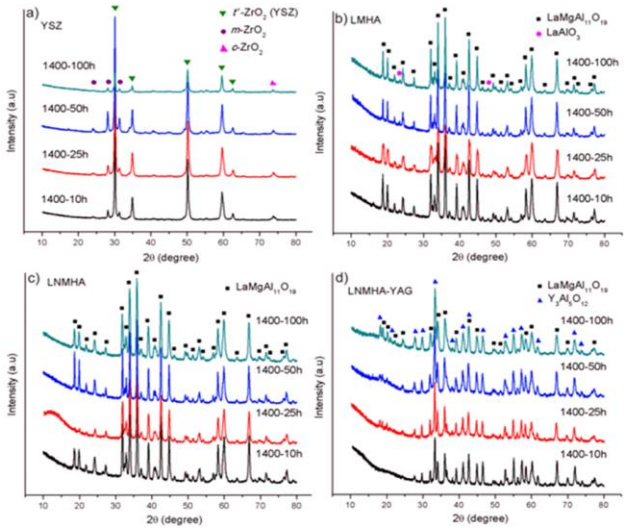

Fig. 6. XRD patterns of isothermally aged free standing coatings: a) YSZ, b) LMHA, c) LNMHA and d) LNMHA-YAG.

Phase analysis

XRD patterns of isothermally aged free standing coatings are shown in **Fig. 6**. There is a significant degradation of YSZ coating. The trace monoclinic phase which was present in the as sprayed coatings **(Fig. 2a)** becomes a significant phase after isothermal aging at 1400 °C for 100 h **(Fig. 6a)**. The monoclinic phase content is calculated based on the equation 2 and given in **Table 3**.

Table 3. The monoclinic phase content of isothermally aged YSZ coating.

Phase content	1400°C-10h	1400°C - 25h	1400°C - 50h	1400°C-100h
% m-ZrO_2 phase	7.09	9.35	23.06	25.48

$$\%\, m\text{–}ZrO_2 = \frac{I_m(\bar{1}11)+I_m(111)}{I_m(\bar{1}11)+I_m(111)+I_{t'}(111)} \times 100 \qquad (2)$$

where, I is the diffraction peak intensity of the respective planes.

The metastable tetragonal phase (t'-ZrO_2) converts into equilibrium tetragonal and cubic phases by the diffusion of Y^{3+} at elevated temperature and the equilibrium tetragonal phase transforms into monoclinic phase during cooling to room temperature. As a result, the monoclinic phase is present along with the metastable tetragonal phase.

The phases of hexaaluminate based coatings remain intact even after 100 h of isothermal aging at 1400 °C. The trace of lanthanum mono aluminate phase is also present in case of LMHA coatings. Almost phase pure lanthanum magnesium hexaaluminate is observed in LNMHA coating and remains same even after 100 h. Similar phenomenon is observed for LNMHA-YAG coating, i.e., the LMHA and YAG phases remain unaffected.

Microstructural analysis

The microstructural changes of isothermally aged YSZ coating is shown in **Fig. 7**. The microstructure of isothermally aged YSZ coating reveals that severe sintering and grain growth take place during the isothermal treatment. The lamellae are well crystallized and the grain grows progressively as a function of dwelling time. The columnar grain structure of as sprayed YSZ coating is changed to a spherical, equiaxed grain by the isothermal treatment. Few equiaxed grains are grown excessively than the matrix, i.e., abnormal grain growth is more prominent as the dwelling time increased. The excessive sintering results in higher relative density as discussed in earlier section (3.1.4).

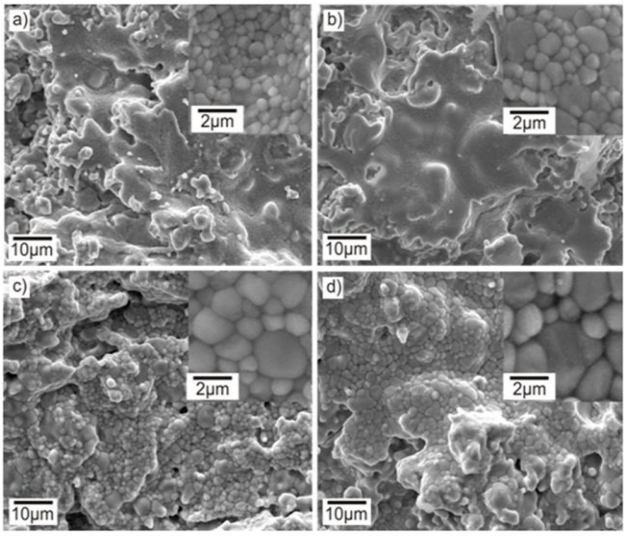

Fig. 7. Microstructure of isothermally aged YSZ coating at 1400°C with a dwelling time of a) 10 h, b) 25 h, c) 50 h and d) 100 h.

The microstructure of isothermally aged LMHA coating is shown in **Fig. 8**. The as sprayed LMHA coating is amorphous in nature and gets crystallized during heat treatment. The platelets of lanthanum magnesium hexaaluminate are well grown after 10 h of dwelling time **(Fig. 8a)** and almost remain unaltered even after 25 h of holding **(Fig. 8b)**. The platelets start growing faster as the dwelling time increased further (>25 h) but the platelet morphology remains unaffected and grows uniformly. The crystallization and sintering of amorphous coating cause volumetric shrinkage that leads to development of few micro cracks in the coating **(Fig. 8c)**. Generally, the presence of micro cracks on the coatings helps to dissipate the strain energy during thermal cycling.

Copyright © 2018 VBRI Press

Therefore, the amorphous hexaaluminate based coating may have inherent advantages of generating micro cracks during crystallization which can lead to better TBC life.

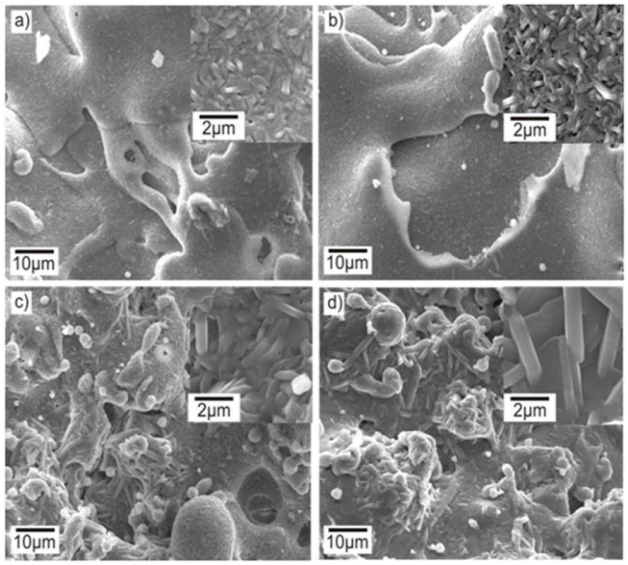

Fig. 8. Microstructure of isothermally aged LMHA coating at 1400 °C with a dwelling time of a) 10 h, b) 25 h, c) 50 h and d) 100 h.

The microstructure of isothermally aged LNMHA coating is shown in **Fig. 9**. The amorphous coating gets well crystallized at 1400 °C after holding for 10 h **(Fig. 9a).** It also has platelets morphology like LMHA coating. The grain growth rate is reasonably low till 50 h of dwelling and then increases faster **(Fig. 9d)**. However the final platelet size is relatively smaller than that of LMHA coatings when compared after 100 h of holding **(Fig. 8d** and **9d).** The sintering resistance of this coating seems to be better than YSZ coating and comparable with the LMHA coating. Few micro cracks are present after 50 h **(Fig. 9c)** and 100 h **(Fig. 9d)** of dwelling that can be attributed to the shrinkage due to the crystallization and sintering of the coating.

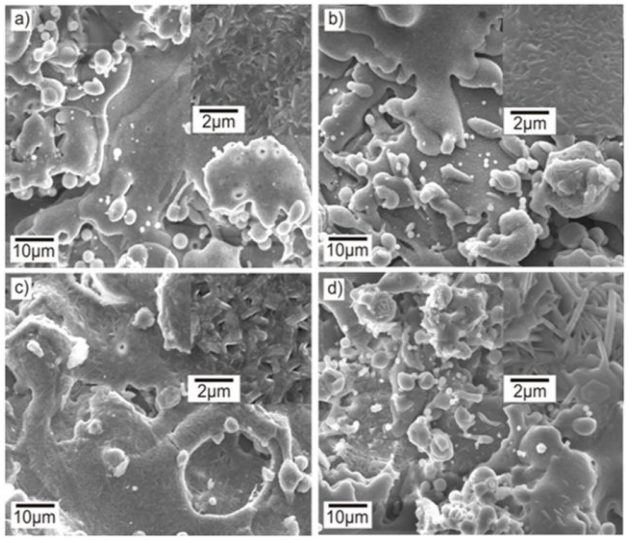

Fig. 9. Microstructure of isothermally aged LNMHA coating at 1400 °C with a dwelling time of a) 10 h, b) 25 h, c) 50 h and d) 100 h.

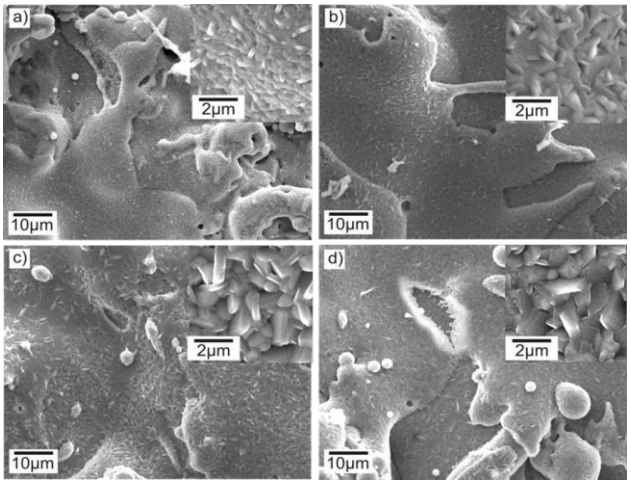

Fig. 10. Microstructure of isothermally aged LNMHA-YAG coating at 1400 °C with a dwelling time of a) 10 h, b) 25 h, c) 50 h and d) 100 h.

The microstructural characteristics of isothermally aged LNMHA-YAG composite coating are shown in **Fig. 10**. The amorphous coating gets crystallized nicely and the platelets of LMHA as well as spherical YAG crystals are clearly evident. The LMHA and YAG crystals are well distributed as observed for the bulk sample. The growth of both type of grains are progressively increased with the increment of dwelling time. The grain boundaries between two different grains are very intact even after 100 h of dwelling **(Fig. 15d)**. The sintering of this coating is not as severe as seen for YSZ coating but relatively higher than the LNMHA coating.

Grain growth characteristics

The plot of grain size as a function of soaking time of isothermally aged four different coatings is shown in **Fig. 11a**. The best fitted curves show that the growth characteristics of YSZ as well as hexaaluminate based coatings follow the parabolic growth law. The YSZ coating is having higher growth rate than that of hexaaluminate based coatings. The LMHA coating has much faster growth rate among the hexaaluminate based coatings whereas LNMHA coating has the lowest growth kinetics. The LNMHA-YAG composite coating has little higher growth rate than the LNMHA coating. The Bruke and Turnbull's kinetic equation for isothermal grain growth is expressed in equation 3 [31, 32].

$$D^n - D_o^n = Kt \quad (3)$$

where, D_o and D are the initial and final grain size after dwelling time t, respectively, K is a temperature dependent rate constant and follow Arrhenius type equation, n is the grain growth exponent. For an ideal single phase system, n is equal to 2.

Since the plasma sprayed hexaaluminate based coatings are amorphous and YSZ coating is also fine crystalline, one can consider $D >> D_o$. Therefore, the equation 3 can be rewritten as:

$$D^n = Kt \text{or} D = K' t^{\frac{1}{n}} \quad (4)$$

Copyright © 2018 VBRI Press

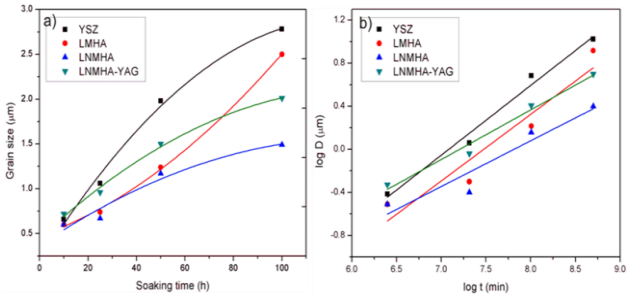

Fig. 11. (a) The plot of grain size as a function of soaking time and (b) the plot of *log D*vs*log t* of four different TBCs.

The grain growth exponent can be obtained from the plot of *log D*vs*log t* as shown in **Fig. 11b**. The value of *n* for different coatings are calculated and summarized in **Table 4**. The highest n value is seen for the LNMHA coatings and the lowest for the YSZ coatings. From the equation 4, it is clear that lower the exponent (*n*), higher the grain growth rate. Therefore, YSZ is more prone to grow with dwelling time whereas LNMHA is the most grain growth resistant. The ascending order of grain growth resistance is YSZ<LMHA<LNMHA-YAG<LNMHA.

Table 4. The grain growth exponent.

Type of TBCs	YSZ	LMHA	LNMHA	LNMHA-YAG
Grain growth exponent (n)	1.54	1.61	2.53	2.17

Micro-hardness of isothermally aged TBCs

The variation of micro hardness of isothermally aged free standing coatings is shown in **Fig. 12**. The hardness measurement is performed on the coating surface after mounting and polishing. The hardness of YSZ coating shows a significant drop from 11.74±0.43 GPa to 7.53±0.31 GPa, whereas hexaaluminate based coatings have marginal drop in hardness. The hardness of LMHA coating has reduced more among the hexaaluminate based coatings.

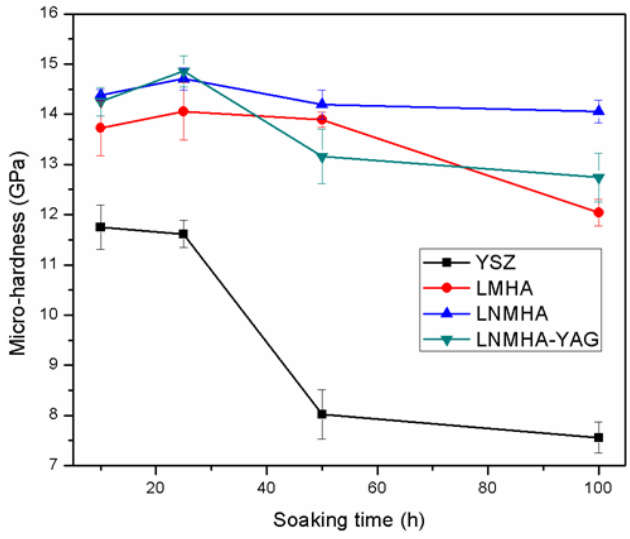

Fig. 12. Micro-hardness of isothermally aged free standing coatings.

The drop in hardness can be explained from the grain size of the materials. The well-known Hall-patch equation explains the inter relation between the hardness and grain size. The hardness is inversely proportional to the grain size, i.e., higher the grain size, lower the hardness. The grain growth characteristics are discussed in previous section (3.2.3). There is a substantial grain growth for YSZ and LMHA coatings with increase in dwelling time thus causing larger drop in hardness. The monoclinic phase content of YSZ coating can also influence such reduction. The LNMHA and LNMHA-YAG composite coatings have shown marginal grain growth even after 100 h and thus causing marginal drop in hardness. The variation in hardness is an indication of TBC's degradation at elevated temperature. Therefore, the LNMHA and LNMHA-YAG composite coatings are less prone to degradation at 1400 °C and almost stable over a longer duration (up to 100h).

Conclusion

Free standing coating of YSZ, LMHA, LNMHA and LNMHA-YAG composite are formed on graphite block by the atmospheric plasma spraying. The porosity level of these TBCs is around 15%. The hexaaluminate based coatings are found to be amorphous in nature whereas YSZ based coatings are well crystalline. The hexaaluminate based coatings get crystallized during heat treatment and form desired phases at 1400 °C for 2 h.

The isothermal aging characteristics of these coatings are performed at 1400 °C for 100 h. The excessive sintering, densification and phase changes are primary reasons for YSZ coating degradation. The excessive grain growth is also seen which resulting in significant drop in hardness. On the other hand, the hexaaluminate based coatings are found to be more sintering and grain growth resistant. Phases of hexaaluminate based coatings are also remained unaltered and demonstrated better thermal stability. The density and hardness of them are remained at decent level even after 100 h of dwelling. The LNMHA coating is found to have the best isothermal aging characteristics. The LNMHA and LNMHA-YAG composite are the potential candidates for advanced thermal barrier coating operating even at 1400 °C.

Acknowledgements

The authors would like to thank M/s Carborundum Universal Limited, India for sponsoring this research work and M/s Sai Surface Coating Technology, Hyderabad, India for providing plasma spraying facility to prepare TBC.

Author's contributions

Conceived the plan: KB, SM; Performed the expeirments: PJ, PSJ; Data analysis: PJ, SM, KB; Wrote the paper: PJ, KB. Authors have no competing financial interests.

References

1. Padture, N. P.; Gell, M.; Jordan, E. H., *Science***2002**, *296*, 280.
2. Vassen, R.; Jarligo, M. O.; Steinke, T.; Mack, D. E.; Stover, D., *Surf. Coat. Technol.***2010**, *205*, 938.
3. Hardwicke, C.; Lau, Y.-C., *J. Therm. Spray Technol.***2013**, *22*, 564.
4. Rajendran, R., *Engineering Failure Analysis***2012**, *26*, 355.

Copyright © 2018 VBRI Press

5. Joulia, A.; Vardelle, M.; Rossignol, S., *J. Eur. Ceram. Soc.***2013**, *33*, 2633.
6. Vassen, R.; Traeger, F.; Stover, D., *International Journal of Applied Ceramic Technology***2004**, *1*, 351.
7. Boyce, M. P., *Gas Turbine Engineering Handbook*, Butterworth-Heinemann, USA **2012**.
8. Xiaoge, C.; Shusen, Y.; Hongsong, Z.; Gang, L.; Zhenjun, L.; Bo, R.; Xudan, D.; Haoming, Z.; An, T., *Mater. Res. Bull.***2014**, *51*, 171.
9. Cao, X. Q.; Vassen, R.; Stoever, D., *J. Eur. Ceram. Soc.***2004**, *24*, 1.
10. Guo, L.; Guo, H.; Peng, H.; Gong, S., *J. Eur. Ceram. Soc.***2014**, *34*, 1255.
11. Gadow, R.; Lischka, M., *Surf. Coat. Technol.***2002**, *151-152*, 392.
12. Zhu, R.-X.; Liu, Z.-G.; Ouyang, J.-H.; Zhou, Y., *Ceram. Int.***2013**, *39*, 8841.
13. Bansal, N. P.; Zhu, D., *Surf. Coat. Technol.***2008**, *202*, 2698.
14. Friedrich, C.; Gadow, R.; Schirmer, T., *J. Therm. Spray Technol.***2001**, *10*, 592.
15. Guo, S.; Kagawa, Y., *Ceram. Int.***2007**, *33*, 373.
16. Zhao, X.; Wang, X.; Xiao, P., *Surf. Coat. Technol.***2006**, *200*, 5946.
17. Preauchat, B.; Drawin, S., *Surf. Coat. Technol.***2001**, *146-147*, 94.
18. Schulz, U., *J. Am. Ceram. Soc.***2000**, *83*, 904.
19. Di Girolamo, G.; Blasi, C.; Schioppa, M.; Tapfer, L., *Ceram. Int.***2010**, *36*, 961.
20. Jana, P.; Jayan, P. S.; Mandal, S.; Biswas, K., *J. Mater. Sci.***2015**, *50*, 344.
21. Jana, P.; Jayan, P. S.; Mandal, S.; Biswas, K., *Mater. Lett.***2015**, *145*, 321.
22. Jana, P.; Jayan, P. S.; Mandal, S.; Biswas, K., *J. Cryst. Growth***2014**, *408*, 7.
23. Anstis, G. R.; Chantikul, P.; Lawn, B. R.; Marshall, D. B., *J. Am. Ceram. Soc.***1981**, *64*, 533.
24. Marshall, D. B.; Noma, T.; Evans, A. G., *J. Am. Ceram. Soc.***1982**, *65*, c175.
25. Chen, X.; Zou, B.; Wang, Y.; Ma, H.; Cao, X., *J. Therm. Spray Technol.***2011**, *20*, 1328.
26. Chen, X.; Zhao, Y.; Huang, W.; Ma, H.; Zou, B.; Wang, Y.; Cao, X., *J. Eur. Ceram. Soc.***2011**, *31*, 2285.
27. Beshish, G.; Florey, C.; Worzala, F.; Lenling, W., *J. Therm. Spray Technol.***1993**, *2*, 35.
28. Seiler, P.; Baker, M.; Rosler, J., *Computational Materials Science***2013**, *80*, 27.
29. Wu, J.; Guo, H.-b.; Gao, Y.-z.; Gong, S.-k., *J. Eur. Ceram. Soc.***2011**, *31*, 1881.
30. Vassen, R.; Sebold, D.; Stöver, D., in *Advanced Ceramic Coatings and Interfaces II: Ceramic and Engineering Science Proceedings, Volume 28, Issue 3*, John Wiley & Sons, Inc., **2009**, 27.
31. Lai, J. K. L.; Shek, C. H.; Lin, G. M., *Scripta Mater.***2003**, *49*, 441.
32. Gil, F. X.; Rodriguez, D.; Planell, J. A., *Scripta Metallurgica et Materialia***1995**, *33*, 1361.

Copyright © 2018 VBRI Press